Velocity Pointing Errors Associated with Spinning Thrusting Spacecraft

Daniel Javorsek II* and James M. Longuski†
Purdue University, West Lafayette, Indiana 47907-1282

Because of the imperfection of spacecraft assembly, there always exist misalignment and offset torques during thrust maneuvers. In the case of an axially thrusting spin-stabilized spacecraft, these torques disturb the angular momentum vector in inertial space causing a velocity pointing error. Much insight can be gained by analytically solving the problem of time-varying torques and time-varying moments of inertia. We use approximate analytic solutions to suggest how the velocity pointing error can be reduced for some practical assumptions based on current technology. For example, in the case of solid rocket motors, a significant improvement in velocity pointing can be realized by judicious distribution of the propellant.

Nomenclature

a	=	acceleration, m/s^2
C	=	Fresnel cosine
d	=	offset distance, m
F	=	thrust, N
H	=	angular momentum, kg-m^2/s
h	=	distance from throat of nozzle to the center of mass, m
I	=	principal moment of inertia, kg-m^2
$\mathfrak{J}$	=	impulse, kg-m/s
M	=	moment, Nm
m	=	mass, kg
$\dot{m}$	=	mass-flow rate, kg/s
S	=	Fresnel sine
t	=	time, s
α	=	misalignment angle, deg
γ	=	angle between actual velocity vector and desired velocity vector, deg
ΔV	=	velocity change, m/s
ε	=	error
ρ	=	angle between average angular momentum vector and inertial Z axis, deg
ϕ	=	Euler angles, deg
Ω	=	initial spin rate, rad/s
ω	=	angular velocity, rad/s

Subscripts

b	=	total burn, used to distinguish the total burn time
f	=	final state
r	=	ramp, used to distinguish ramp times
X, Y, Z	=	orthogonal inertially fixed coordinates
x, y, z	=	orthogonal body-fixed coordinates
0	=	initial state

Introduction

IT is impossible to build an ideal thrusting mechanism in a real spacecraft. Various anomalies, such as thruster misalignment or center-of-mass offset, will create body-fixed torques transverse to the spin axis. An example of such a configuration is shown in Fig. 1 (where d and α are exaggerated for clarity). We restrict our analysis to the case of an axially thrusting spin-stabilized spacecraft, where

transverse torques perturb the angular momentum vector $\boldsymbol{H}$ from its original direction and induce a velocity pointing error.

Longuski et al.[1] investigate the thrusting spinning spacecraft for constant body-fixed torques and constant moments of inertia and demonstrate that the angular momentum vector and the velocity vector are offset in inertial space by the same bias angle. We address a related problem and begin our analysis by obtaining approximate analytical solutions for two different cases: 1) time-varying torque with constant moments of inertia and 2) constant torque with a time-varying moment of inertia. Each of these approximate analytical solutions provides insight into how velocity pointing error can be reduced significantly with a prescribed thrust profile.

In case 1 we study linearly changing body-fixed torques and their impact on the behavior of the angular momentum vector. This case applies to short duration burns where the inertia properties remain nearly constant. In case 2 we consider the common spacecraft dynamics problem in which a significant amount of propellant is consumed (such as in the case of an upper-stage injection of a satellite into geostationary or escape orbit). Case 2 also addresses the motion of the angular momentum vector in inertial space. The solutions derived in each case permit us to piece together an approximate analytical solution for the angular momentum vector behavior for a particular thrust profile. Based on the analytic solution, we prescribe a thrust profile that minimizes the angular momentum pointing error. In a high-fidelity case study we show that the resulting velocity pointing error is significantly less than that achieved with a conventional thrust profile.

Figure 1 illustrates the problem configuration, where $h(t)$ is the vertical distance from the point of the force application to the center of mass (CM) and $F(t)$ is the thrust.

Analytic Solutions

Case 1: Constant Moment of Inertia with Time-Varying Torque

Simple Model for the Angular Momentum Vector

We will work directly with Euler's law about the CM:

$$M = \frac{\mathrm{d}\boldsymbol{H}}{\mathrm{d}t} \qquad (1)$$

By assuming a nearly symmetric spacecraft with no axial torque, the spin rate Ω will be constant. Furthermore, to eliminate the complications of solving for the attitude motion (e.g., Euler angles) we assume the transverse body-fixed torque M_x remains in the inertial XY plane. For a symmetric spacecraft we set $M_y = 0$ without loss of generality. For a linearly time-varying M_x in the body xy plane and referring to Fig. 1, we have

$$M_x = F(t)[h(t)\sin\alpha + d\cos\alpha] \qquad (2)$$

or

$$M_x = c_1 t + c_2 \qquad (3)$$

Fig. 1 Spacecraft and rocket configuration.
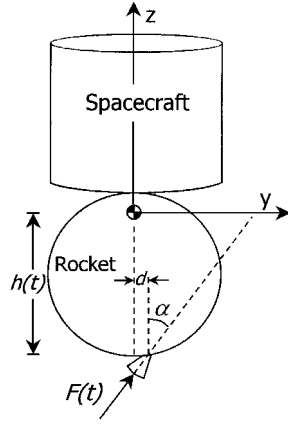
Table 1 Spacecraft and PAM data for numerical simulation

Property	Notation	Quantity
Maximum thrust force	F_{max}	76,100 N
Maximum CM offset	d	0.02 m
Thrust misalignment	α	0.25 deg
Initial distance from throat[a] to CM	h_0	0.80 m
Final distance from throat to CM	h_f	1.55 m
Initial spin rate	Ω_0	70 rpm
Initial PMOI[b] about x axis	I_{x0}	858 kg-m^2
Final PMOI about x axis	I_{xf}	222 kg-m^2
Initial PMOI about y axis	I_{y0}	858 kg-m^2
Final PMOI about y axis	I_{yf}	222 kg-m^2
Initial PMOI about z axis	I_{z0}	401 kg-m^2
Final PMOI about z axis	I_{zf}	102 kg-m^2
Mass	m	2,500 kg
Mass-flow rate	$\dot{m}$	−24 kg/s

[a]Throat of the nozzle for the motor.   [b]Principal moment of inertia.

From these assumptions Eq. (1) can be written as

$$\dot{H}_X = M_X = (c_1 t + c_2)\cos\Omega t \qquad (4)$$

$$\dot{H}_Y = M_Y = (c_1 t + c_2)\sin\Omega t \qquad (5)$$

$$\dot{H}_Z = M_Z = 0 \qquad (6)$$

$$\begin{bmatrix} H_X \\ H_Y \\ H_Z \end{bmatrix} = \begin{bmatrix} c\phi_x c\phi_z - s\phi_x s\phi_y s\phi_z & -s\phi_x c\phi_y & c\phi_x s\phi_z + s\phi_x s\phi_y c\phi_z \\ s\phi_x c\phi_z + c\phi_x s\phi_y s\phi_z & c\phi_x c\phi_y & s\phi_x s\phi_z - c\phi_x s\phi_y c\phi_z \\ -c\phi_y s\phi_z & s\phi_y & c\phi_y c\phi_z \end{bmatrix} \begin{bmatrix} I_x \omega_x \\ I_y \omega_y \\ I_z \omega_z \end{bmatrix} \qquad (16)$$

For the initial conditions $H_X(0) = H_Y(0) = 0$ and $H_Z(0) = I_z \omega_{z0} = I_z\Omega$, the integration of Eqs. (4–6) provides the following:

$$H_X = \left(c_1\big/\Omega^2\right)\cos\Omega t + [(c_1 t + c_2)/\Omega]\sin\Omega t - c_1\big/\Omega^2 \quad (7)$$

$$H_Y = \left(c_1\big/\Omega^2\right)\sin\Omega t - [(c_1 t + c_2)/\Omega]\cos\Omega t + c_2\big/\Omega \quad (8)$$

$$H_Z = I_z\Omega \qquad (9)$$

The assumption that M_X remains in the inertial XY plane has serious limitations and must be applied with caution. To check our heuristic solution for the angular momentum behavior, we apply a more formal approach starting with Euler's equations of motion.[1]

Outline of Formal Solution for the Angular Momentum Vector

For time-varying torques and constant principal moments of inertia, Euler's equations of motion are

$$M_x = I_x \dot{\omega}_x + (I_z - I_y)\omega_y\omega_z \qquad (10)$$

$$M_y = I_y \dot{\omega}_y + (I_x - I_z)\omega_z\omega_x \qquad (11)$$

$$M_z = I_z \dot{\omega}_z + (I_y - I_x)\omega_x\omega_y \qquad (12)$$

Assuming a near symmetric rigid body $I_x \approx I_y$ under the influence of a single time-varying torque M_x, the spin rate is nearly constant with time (i.e., $\omega_z \approx \omega_{z0} = \Omega$). The solutions of Euler's equations of motion are relatively insensitive to variations in I_x and I_y if the orientation changes in H are small.[2,3]

There are 12 forms of Euler-angle rotation representations to give the attitude of a spacecraft. If a type 1: 3-1-2 rotation is used,[4] the kinematic equations are

$$\dot{\phi}_x = (\omega_z \cos\phi_z - \omega_x \sin\phi_z)\sec\phi_y \qquad (13)$$

$$\dot{\phi}_y = \omega_x \cos\phi_z + \omega_z \sin\phi_z \qquad (14)$$

$$\dot{\phi}_z = \omega_y + (\omega_x \cos\phi_z + \omega_z \sin\phi_z)\tan\phi_y \qquad (15)$$

For small ϕ_x and ϕ_y an analytic solution is obtained[5] for the case of near symmetric rigid bodies with constant body-fixed torques.

When analytic expressions are available for Euler's equations of motion and the preceding Eulerian angles, the angular momentum vector in inertial space can be evaluated using

where c and s denote the cosine and sine. This relationship may be simplified for small angles.

Comparison of Analytical Solution with Numerical Results

Equations (7–9) indicate that the angular momentum vector follows a spiral path in space (as shown in Fig. 2a). We have verified our heuristic approach, by performing a highly precise numerical integration of Eqs. (10–15) and using Eq. (16). (For the numerical values represented in Table 1, the maximum error between the heuristic and the numerically integrated solutions is around 3.6×10^{-3} mrad.)

Case 2: Time-Varying Moment of Inertia with Constant Torque
Simple Model for the Angular Momentum Vector

Again we use Euler's law

$$\boldsymbol{M} = \frac{d\boldsymbol{H}}{dt} \qquad (17)$$

This time we cannot assume the spin rate is constant. To make the equations integrable, a constant transverse torque M_x is assumed (with $M_y = 0$). To simplify the approximate analytical solution, we neglect jet damping. For the case of generalized torques and a variable moment of inertia, Euler's third equation of motion becomes

$$M_z = \dot{I}_z(t)\omega_z(t) + I_z(t)\dot{\omega}_z(t) + (I_y - I_x)\omega_x\omega_y \qquad (18)$$

For a nearly symmetric rigid body Eq. (18) becomes

$$M_z = \dot{I}_z(t)\omega_z(t) + I_z(t)\dot{\omega}_z(t) = \frac{d}{dt}[I_z(t)\omega_z(t)] \qquad (19)$$

Assuming no z-axis torque ($M_z = 0$), Eq. (19) indicates that $I_z(t)\omega_z(t)$ is constant. Therefore, H_Z is conserved and remains constant in inertial space with the magnitude

$$H_Z = I_z(0)\omega_z(0) = I_z(t)\omega_z(t) \qquad (20)$$

As a result, when I_z changes, the spin rate must also change to conserve H_Z by the following equation:

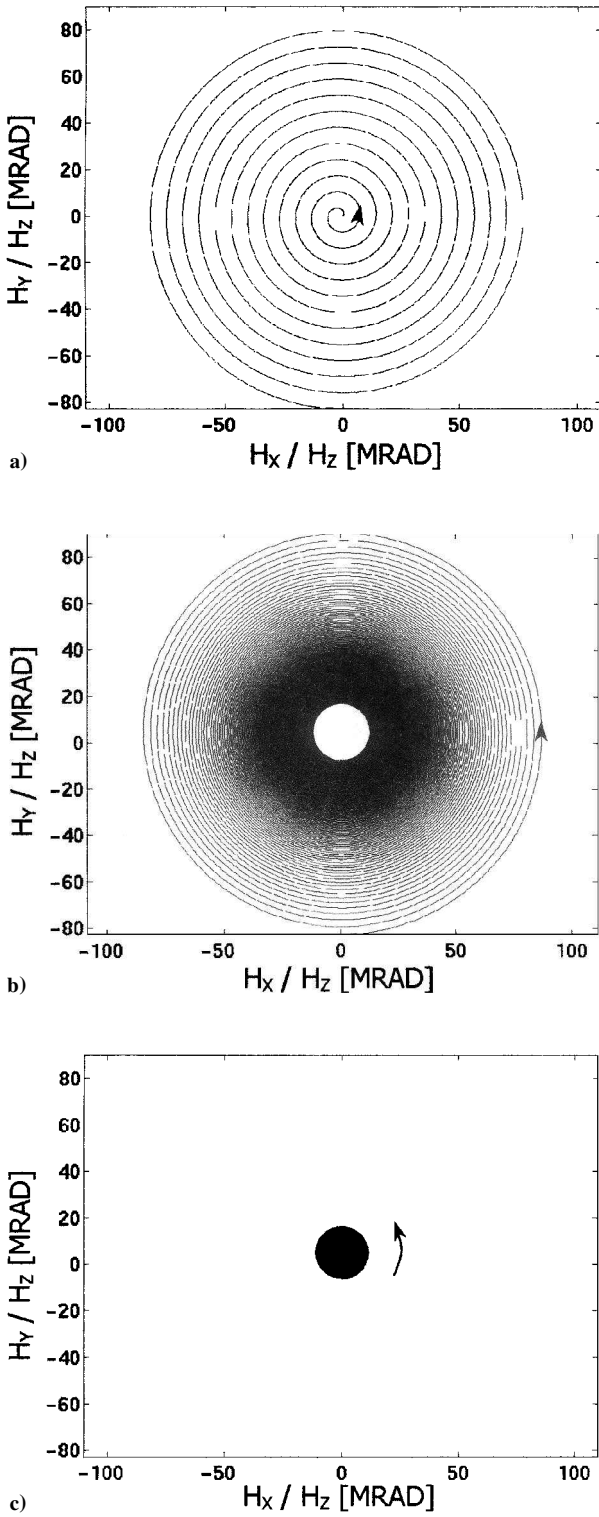$$\omega_z(t) = H_Z/I_z(t) = I_{z0}\Omega/I_z(t) \qquad (21)$$

Fig. 2 Analytical solution to the angular momentum vector in inertial space for phase a) 1, b) 2, and c) 3 of the trapezoidal thrust scheme.

Using the heuristic approach, Euler's law results in the following:

$$\dot{H}_X = M_X = M_x \cos\left\{ \int_0^t \left(\frac{I_{z0}\Omega}{I_z(t)} \right) dt \right\} \tag{22}$$

$$\dot{H}_Y = M_Y = M_x \sin\left\{ \int_0^t \left(\frac{I_{z0}\Omega}{I_z(t)} \right) dt \right\} \tag{23}$$

$$\dot{H}_Z = 0 \tag{24}$$

Equations (22) and (23) are integrable in terms of Fresnel integrals if

$$\int_0^t \left(\frac{I_{z0}\Omega}{I_z(t)} \right) dt = at^2 + bt + c$$

$$= at^2 + \Omega t \tag{25}$$

This implies that

$$I_z(t) = I_{z0}/(2at/\Omega + 1) \tag{26}$$

For small values of $2at/\Omega$, Eq. (26) can be approximated by

$$I_z(t) = I_{z0}(1 - 2at/\Omega) \tag{27}$$

so that I_z decreases linearly as a function of time. For the initial conditions $H_X(0) = H_Y(0) = 0$, and $H_Z(0) = I_{z0}\Omega$, the integration of Eqs. (22–24) provides

$$H_X = M_x \sqrt{\frac{\pi}{a}} \left\{ \cos\left(\frac{\Omega^2}{2a}\right) C\left[\sqrt{\frac{4}{a\pi}} \left(\frac{at + \Omega}{2} \right) \right] \right.$$

$$\left. + \sin\left(\frac{\Omega^2}{2a}\right) S\left[\sqrt{\frac{4}{a\pi}} \left(\frac{at + \Omega}{2} \right) \right] \right\} \tag{28}$$

$$H_Y = M_x \sqrt{\frac{\pi}{a}} \left\{ \cos\left(\frac{\Omega^2}{2a}\right) S\left[\sqrt{\frac{4}{a\pi}} \left(\frac{at + \Omega}{2} \right) \right] \right.$$

$$\left. - \sin\left(\frac{\Omega^2}{2a}\right) C\left[\sqrt{\frac{4}{a\pi}} \left(\frac{at + \Omega}{2} \right) \right] \right\} \tag{29}$$

$$H_Z(t) = I_{z0}\Omega \tag{30}$$

The Fresnel integrals in Eqs. (28) and (29) can be approximated as follows[6]:

$$C(z) = \frac{1}{2} + f(z) \sin\left(\frac{\pi}{2} z^2\right) - g(z) \cos\left(\frac{\pi}{2} z^2\right)$$

$$S(z) = \frac{1}{2} - f(z) \cos\left(\frac{\pi}{2} z^2\right) - g(z) \sin\left(\frac{\pi}{2} z^2\right)$$

$$f(z) = \frac{1 + 0.926(z)}{2 + 1.792(z) + 3.104(z^2)} + \varepsilon(z), \qquad |\varepsilon(z)| \leq 2 \times 10^{-3}$$

$$g(z) = \frac{1}{2 + 4.142(z) + 3.492(z^2) + 6.670(z^3)} + \varepsilon(z)$$

$$|\varepsilon(z)| \leq 2 \times 10^{-3} \tag{31}$$

For a more accurate representation ($|\varepsilon| \leq 10^{-9}$), see Ref. 7.

Comparison of Analytical Solution with Numerical Results

A sample plot of the inertial angular momentum components represented by Eqs. (28–30) is shown in Fig. 2b. As in case 1, we tested our heuristic approach against numerical integration. (The values provided in Table 1 result in a difference between the two solutions of 4.2×10^{-2} mrad.)

Thrusting Maneuvers

Construction of an Analytic Solution for the Trapezoidal Thrust Scheme

We wish to produce a thrust profile to minimize velocity pointing error while simultaneously driving the angular momentum vector back to its initial position. Our goal is to maintain the average orientation of **H** along the initial inertial **Z** direction, which is the desired

Table 2 Summary of each phase of the trapezoidal thrust scheme

Phase	Thrust	I_z	Distance to CM	Mass	Invariant constants
1	Linearly increasing	I_{z0}	h_0	m_0	I_x, I_y, d, α
2	$F_{\max}$	Linearly decreasing	$(h_0 + h_f)/2$	$(m_0 + m_f)/2$	I_x, I_y, d, α
3	Linearly decreasing	I_{zf}	h_f	m_f	I_x, I_y, d, α
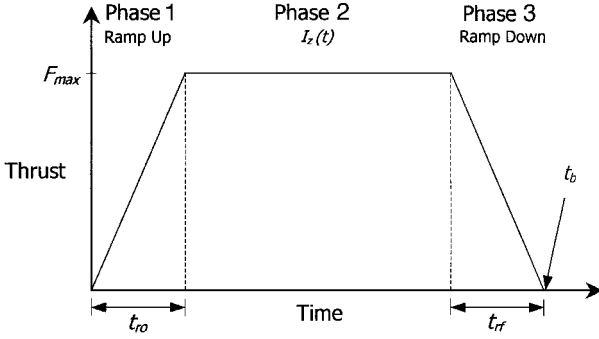
Fig. 3 Sample thrust profile of the trapezoidal thrust scheme.

direction of the ΔV. Even though H moves around in inertial space, if its average orientation is along Z, the velocity vector will tend to align along Z as well. The trapezoidal thrust profile shown in Fig. 3 accomplishes the goal of maintaining the average H along Z. Piecing together the solutions already derived for each segment of the profile creates the corresponding analytical solution for the angular momentum vector.

In general, a spacecraft has principal moments of inertia and mass properties that are changing with time. In the trapezoidal thrust scheme we always assume that $\dot{m}$ and h are constant (where average values are used for the constants). The thrust increases linearly over the first phase of the burn. Because this phase is short compared to the entire burn time, we assume constant principal moments of inertia in the analytic solution. During the second phase, the thrust is held constant, and the principal moment of inertia associated with the axis of symmetry decreases linearly. The burn time of the third and final phase is shorter than that of the first phase because of the increased spin rate that results from the decreasing I_z in phase 2. Again we assume constant moments of inertia while the thrust decreases linearly (Table 2).

It is not necessary that the thrust profile be entirely symmetrical. Because the spin rate is increasing throughout the burn, t_{rf} will not have to be as long as t_{r0} in order to obtain the same results. However, each of them will be dependent on the spin rate Ω with the following relationship:

$$t_r > n(2\pi/\Omega) \tag{32}$$

where n is some integer. For the ideal case when the initial and final spin rates are known exactly, $n = 1$ will permit minimized pointing errors and will result in a final angular momentum vector position coincident with the initial position. In practice, however, we never obtain the precise spin rate we desire. Thus, depending on the amount of uncertainty we have in the spin rate, the value for n should be greater than one. The sensitivity of the velocity pointing error to uncertainty in spin rate decreases as n increases. In our numerical example (Fig. 2a) we use a value for n of 12, which results in the angular momentum vector making 12 intermediate spirals on the initial ramping portion of the trapezoidal thrust scheme (phase 1).

Thus, the analytical solution for the trapezoidal thrust scheme results in a combination of the preceding solutions and can be represented by the following equations.

Phase 1, $t < t_{r0}$:

$$H_X = (h_0 \sin\alpha + d\cos\alpha)(F_{\max}/t_{r0}\Omega_0)[(1/\Omega_0)\cos(\Omega_0 t)$$

$$+ t\sin(\Omega_0 t) - 1/\Omega_0]$$

$$H_Y = (h_0 \sin\alpha + d\cos\alpha)(F_{\max}/t_{r0}\Omega_0)[(1/\Omega_0)\sin(\Omega_0 t)$$

$$- t\cos(\Omega_0 t)]$$

$$H_Z = I_{Z0}\Omega_0 \tag{33}$$

Phase 2, $t_{r0} < t < t_b - t_{\mathrm{rf}}$:

$$H_X = M_{x\,\max}\sqrt{\frac{\pi}{a}}\left(\cos\left(\frac{\Omega_0^2}{2a}\right)C(z) + \sin\left(\frac{\Omega_0^2}{2a}\right)S(z)\right)$$

$$H_Y = M_{x\,\max}\sqrt{\frac{\pi}{a}}\left(\cos\left(\frac{\Omega_0^2}{2a}\right)S(z) - \sin\left(\frac{\Omega_0^2}{2a}\right)C(z)\right)$$

$$H_Z = I_{z0}\Omega_0 \tag{34}$$

where

$$M_{x\,\max} = F_{\max}(h_{\mathrm{avg}}\sin\alpha + d\cos\alpha)$$

$$a = \frac{\Omega_0}{(t_b - t_{r0} - t_{\mathrm{rf}})}\left(\frac{I_{z0}}{I_{zf}} - 1\right), \qquad z = \sqrt{\frac{4}{a\pi}}\left(\frac{a(t - t_{r0}) + \Omega_0}{2}\right) \tag{35}$$

Phase 3, $t_b - t_{\mathrm{rf}} < t < t_b$:

$$H_X = (h_f \sin\alpha + d\cos\alpha)(F_{\max}/t_{\mathrm{rf}}\Omega_f)[-(1/\Omega_f)\cos(\Omega_f t)$$

$$+ (t_b - t)\sin(\Omega_f t) - 1/\Omega_f]$$

$$H_Y = (h_f \sin\alpha + d\cos\alpha)(F_{\max}/t_{\mathrm{rf}}\Omega_f)[-(1/\Omega_f)\sin(\Omega_f t)$$

$$- (t_b - t)\cos(\Omega_f t) + t_b]$$

$$H_Z = I_{zf}\Omega_f \tag{36}$$

Velocity Pointing Errors During Thrusting Maneuvers

Let us use the angles ρ_X and ρ_Y to specify the orientation of the angular momentum vector in inertial space:

$$\tan\rho_X = H_X / H_Z \tag{37}$$

$$\tan\rho_Y = H_Y / H_Z \tag{38}$$

The average values of these angles provide an accurate approximation for the velocity pointing error even when M_x and I_z are time varying as in our case.

In general, the velocity change in inertial space during thrusting can be found through integration of the acceleration equations

$$\begin{bmatrix} a_X \\ a_Y \\ a_Z \end{bmatrix} = A \begin{bmatrix} F_x/m \\ F_y/m \\ F_z/m \end{bmatrix} \tag{39}$$

where A is the transformation matrix given in Eq. (16) and F_x, F_y, F_z represent the body-fixed forces.

To define the velocity pointing error, we assume an instantaneous inertial frame moving with the spacecraft where the thrust duration is assumed to be instantaneous. The desired ΔV is along the inertial Z axis, and in practice this is very nearly so. Integrating Eq. (39) provides the components of the velocity change in inertial space, namely ΔV_X, ΔV_Y, and ΔV_Z. We use the transverse velocities ΔV_X and ΔV_Y to define the velocity pointing error angles γ_X and γ_Y:

$$\tan\gamma_X = \Delta V_X / \Delta V_Z \tag{40}$$

$$\tan\gamma_Y = \Delta V_Y / \Delta V_Z \tag{41}$$

where ΔV_X and ΔV_Y are much smaller than ΔV_Z.
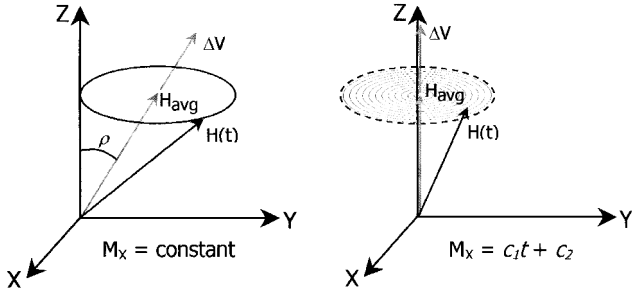
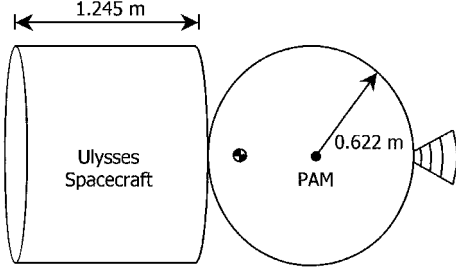Fig. 4 Motion of the angular momentum vector in inertial space for constant and ramp-up thrusts.

Fig. 5 Schematic of generic spacecraft with the PAM.

Because the velocity pointing error is dictated by the average angular momentum vector,[1] we can approximate this error by summing the H vectors from Eqs. (33–36) and dividing by the total burn time. For the trapezoidal thrust scheme this means that we have an analytic solution for the velocity pointing error of the spacecraft. The conclusion is that the trapezoidal thrust scheme keeps the average angular momentum vector along the Z axis. Figure 4 shows this relationship and compares the first phase (the ramp-up segment) of the trapezoidal thrust scheme ($M_x = c_1 t + c_2$) to a step function thrust profile ($M_x = $ constant). When the thrust profile is a step function, the angular momentum vector traces a small circle in inertial space. The average angular momentum vector H_{avg}, lies along the center of this circle, as does the ΔV, which accounts for a velocity pointing error ρ. On the other hand, when the thrust profile is a ramp, the angular momentum vector traces a spiral in inertial space where H_{avg} remains along the desired direction, the Z axis. In this case the ΔV is, to a high degree of accuracy, along the Z axis as well. Thus the velocity pointing error is nearly zero.

We test these analytic solutions in the following case study.

Case Study: Numerical Evaluation of the Payload Assist Module

In our numerical evaluation we study the injection of the Ulysses spacecraft on its interplanetary trajectory to the sun. The spacecraft used the Payload Assist Module (PAM)—more specifically the STAR 48B—to provide a 4.2-km/s velocity increment on 8 October 1990. We use approximate representative values for size, mass, and spin rate of the Ulysses. Humble et al.[8] provide data on the widely used PAM. PAM's nearly spherically symmetric inertia characteristics simplify the analysis. However, this analysis could be performed on any spacecraft and rocket combination given the principal moments of inertia of the system and their time histories. A schematic of the generic spacecraft and rocket system is provided in Fig. 5. The details of the derivations of the mass properties are not included in this paper but can be readily reproduced using the dimensions in the figure and the constants provided in Table 1.

Much of the data in Table 1 was accumulated from Jet Propulsion Laboratory reports,[9] and relative sizes were determined from manufacturers' engine pamphlets. Thrust misalignment is obtained from the excellent work produced by Knauber,[10] which states that most upper-stage fixed nozzle solid rocket motors have a thrust misalignment of less than 0.25 deg.

The first part of the case study is an evaluation of the approximate behavior of the generic system. The model includes linearly
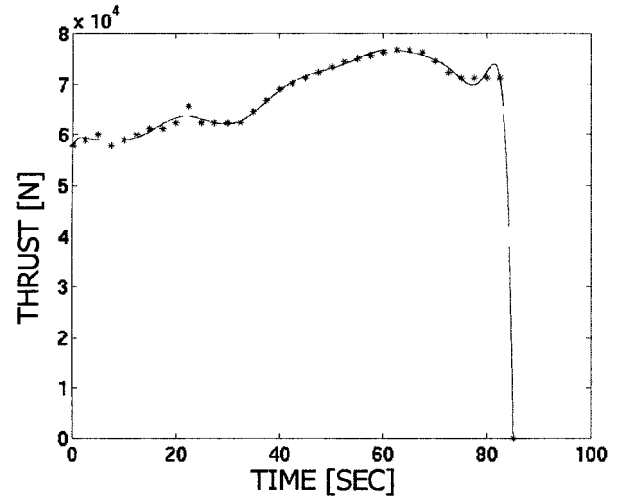
a) Thrust profile
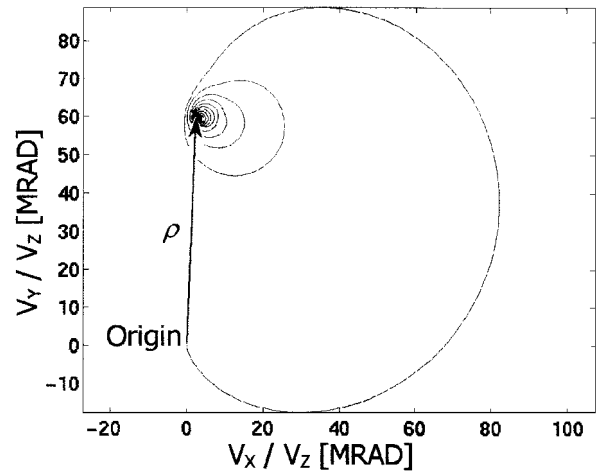
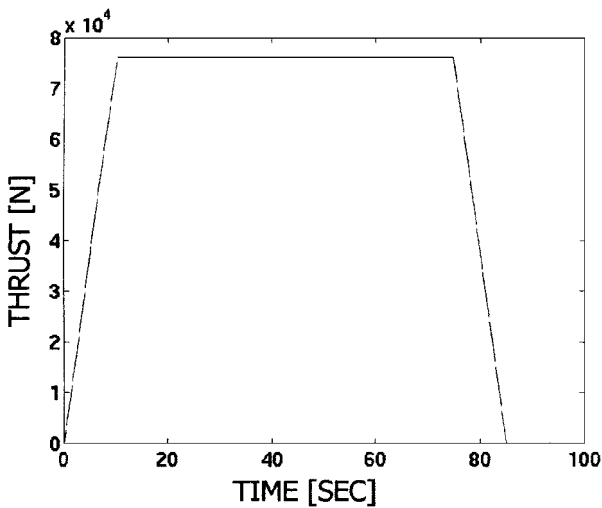b) Velocity pointing error

Fig. 6 Star 48B.

changing principal moments of inertia for all three axes to provide a model that is as accurate as possible. We assume that the CM travels at a constant velocity from the initial to the final positions given in Table 1. The model also assumes a constant mass-flow rate. Finally, unlike the analytical solutions presented before, the higher fidelity model used in the case study includes jet damping.

The CM offset is used as the radius for the jet damping. Following Thomson,[11] we arrive at the equations of motion
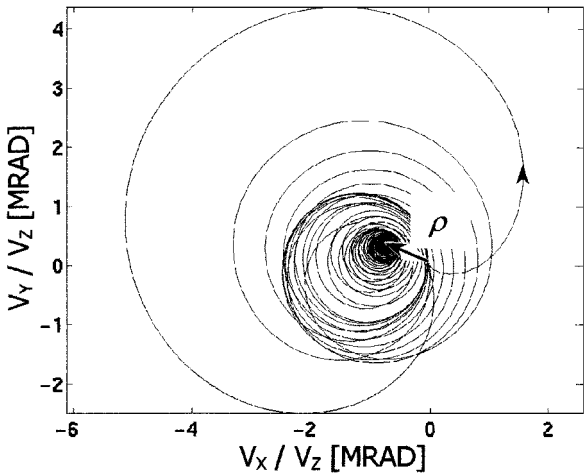
$$M_x = I_x \dot{\omega}_x + \dot{I}_x \omega_x + (I_z - I_y)\omega_y \omega_z - \dot{m}(h^2 + d^2/2)\omega_x$$

$$M_y = I_y \dot{\omega}_y + \dot{I}_y \omega_y + (I_x - I_z)\omega_x \omega_z - \dot{m}h^2 \omega_y$$

$$M_z = I_z \dot{\omega}_z + \dot{I}_z \omega_z + (I_y - I_x)\omega_x \omega_y - \dot{m}d^2 \omega_z \qquad (42)$$

These equations are numerically integrated along with Eqs. (13–15) and Eq. (39) for the Star 48B thrust profile. Data for the Star 48B thrust profile are represented by the 14th-order polynomial curve plotted in Fig. 6a. The subsequent velocity pointing error is shown in Fig. 6b. The average pointing error of 59.5 mrad is also visible in the figure.

Next we analyze the efficacy of the trapezoidal thrust scheme in our case study. To make the comparison as realistic as possible, the burn time, maximum thrust, and total impulse are held constant for both thrust profiles. By working backwards from the known impulse, maximum thrust, and burn time, we are able to calculate the necessary ramp times and to set the rise time of each phase to be $t_{r0} = t_{rf} = t_r$. Using the specification in Eq. (32) with $n = 12$, we confirmed that the computed rise time is large enough for the trapezoidal thrust scheme to prove beneficial.

a) Thrust profile

b) Velocity pointing error

Fig. 7   Trapezoidal thrust scheme.

Table 3   Summary of velocity pointing errors for the case study

Thrust profile	Pointing error, ρ, mrad
Star 48B (Fig. 6a)	59.5
Trapezoidal thrust scheme (Fig. 7a)	0.81

Table 4   Pointing error dependence on model assumptions

Quantity held constant	Velocity pointing error, ρ, mrad
None (case study)	0.811
Without jet damping	0.797
m	0.809
h	0.870
I_x, I_y	0.796
I_z	0.150
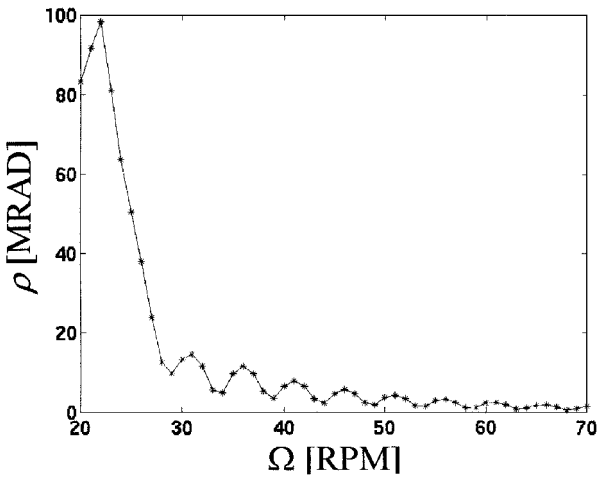
Fig. 8   Velocity pointing error dependence on spin rate for the trapezoidal thrust scheme (case study).

It is very important that the burn time, maximum thrust, and total impulse remain constant between the two comparisons. This requirement is necessary because the PAM is designed to withstand a certain maximum chamber pressure. Because the chamber pressure is proportional to the thrust, the trapezoidal thrust profile cannot exceed the prescribed maximum thrust. The engine is similarly designed to accomplish a specific mission by providing a specific total impulse over a specified burn time. These parameters uniquely specify the engine performance. The ramp time t_r is calculated with the following equation:

$$t_r = t_b - \Im / F_{\max} \qquad (43)$$

The impact of the trapezoidal thrust scheme in our case study is shown in Fig. 7. The only modification is the shape of the thrust profile (Fig. 7a). The velocity pointing error is only 0.81 mrad (Fig. 7b). By comparing Figs. 6b and 7b, we see a drastic decrease in the velocity pointing error. This result is consistent with the goal of maintaining the average angular momentum vector along the Z axis, which is nearly achieved as shown in Figs. (2a–2c). The error predicted by the analytical method [Eqs. (33–36)], based on the average orientation of the angular momentum vector, is 0.58 mrad, which is near the actual value of 0.81 mrad. Table 3 summarizes these results.

From our case study we make a number of observations. First, we note that the thrust profile is dictated by the grain geometry, i.e., how we choose to expose new burn surface area. We can greatly reduce the velocity pointing error by carefully designing the propellant grain geometry. Second, the error committed in our assumptions of

constant I_x, I_y, h_{avg}, and $\dot{m}$ in our analytical analysis is negligible as confirmed by the numerical results. Table 4 provides values for the pointing error when different parameters, which were allowed to vary in the case study, are held constant. The first value listed is the error found in the case study using the trapezoidal thrust scheme, 0.811 mrad. By holding various quantities constant, we see that the variation in I_z has a significant effect on the velocity pointing error.

Finally, in the case of the Ulysses spacecraft, we note that if 60 mrad is an acceptable pointing error then the advantage of using the trapezoidal thrust scheme is that the spacecraft need not be spun up to such a high spin rate. In fact, with the trapezoidal thrust scheme we would only need to spin the spacecraft at 25 rpm instead of the actual 70 rpm used in Ulysses to achieve the same pointing accuracy. For most spin-stabilized spacecraft this is a costly maneuver that must be performed to maintain stability. The benefits are realized again if the spacecraft must be despun after the maneuver. This dependence on spin rate is shown in Fig. 8. The general trend follows the $1/\Omega^2$ law noted in earlier work.[1]

Of course, these models are only approximations of the actual mass and inertia behaviors over time. Many things were not taken into account. We have neglected thermal effects at startup and burnout of the engine and have used an entirely steady-state analysis when performing rocket ballistics. In practice it is difficult to achieve the low thrust levels in phase 1 so that the trapezoidal shape cannot be enforced exactly. Finally, a more practical thrust profile would be similar to that of a trapezoid with rounded corners. In any case, we believe the general statements about the rise time still apply. An interesting follow-on study would be to investigate a grain geometry that permits low initial thrust levels.

Conclusions

1) The velocity pointing error can be closely approximated by the average orientation of the angular momentum vector in inertial space. Approximate analytic solutions for the angular momentum vector are found by directly integrating Euler's law.

2) For a solid rocket motor, by judiciously loading propellant so that the engine thrust profile closely matches a trapezoid, large benefits can be gained in reducing velocity pointing error. This strategy can be employed in other propulsion systems where the thrust profile can be specified.

3) For a given velocity pointing error, the trapezoidal thrust scheme allows for a lower spin rate.

Acknowledgments

References

[1]Longuski, J. M., Kia, T., and Breckenridge, W. G., "Annihilation of Angular Momentum Bias During Thrusting and Spinning-Up Maneuvers," *Journal of the Astronautical Sciences*, Vol. 37, No. 4, 1989, pp. 433–450.

[2]Longuski, J. M., and Kia, T., "A Parametric Study of the Behavior of the Angular Momentum Vector During Spin Rate Changes of Rigid Body Spacecraft," *Journal of Guidance, Control, and Dynamics*, Vol. 7, No. 3, 1984, pp. 295–300.

[3]Kia, T., and Longuski, J. M., "Error Analysis of Analytic Solutions for Self-Excited Near Symmetric Rigid Bodies: A Numerical Study," AIAA Paper 84-2018, Aug. 1984.

[4]Kane, T. R., Likins, P. W., and Levinson, D. A., *Spacecraft Dynamics*, 1st ed., McGraw–Hill, New York, 1983, pp. 422–431.

[5]Longuski, J. M., "Real Solutions for the Attitude Motion of a Self Excited Rigid Body," *Acta Astronautica*, Vol. 25, No. 3, 1991, pp. 131–140.

[6]Abramowitz, M., and Stegun, I. A., *Handbook of Mathematical Functions*, 2nd ed., Dover, New York, 1972, pp. 297–329.

[7]Boersma, J., "Computation of Fresenel Integrals," *Mathematics of Computation*, Vol. 14, No. 72, 1960, p. 380.

[8]Humble, R. W., Henry, G. N., and Larson, W. J., *Space Propulsion Analysis and Design*, 1st ed., Primis Custom Publishing, New York, 1995, pp. 295–360.

[9]Jaffe, P., Diner, A., McRonald, A., and Tenn, L., "Breakup Analysis Final Report," Jet Propulsion Lab., D-1968, 1628-54, California Inst. of Technology, Pasadena, CA, Nov. 1984.

[10]Knauber, R. N., "Thrust Misalignments of Fixed-Nozzle Solid Rocket Motors," *Journal of Spacecraft and Rockets*, Vol. 33, No. 6, 1996, pp. 794–799.

[11]Thomson, W. T., *Introduction to Space Dynamics*, 2nd ed., Dover, New York, 1986, pp. 223–227.

F. H. Lutze Jr.
Associate Editor